

# CaraNet: Context Axial Reverse Attention Network for Segmentation of Small Medical Objects

Ange Lou, Shuyue Guan, Murray Loew

Medical Imaging and Image Analysis Laboratory

Department of Biomedical Engineering

The George Washington University

Washington DC, USA

{angelou, frankshuyueguan, loew}@gwu.edu

## Abstract

Segmenting medical images accurately and reliably is important for disease diagnosis and treatment. It is a challenging task because of the wide variety of objects' sizes, shapes, and scanning modalities. Recently, many convolutional neural networks (CNN) have been designed for segmentation tasks and achieved great success. Few studies, however, have fully considered the sizes of objects and thus most demonstrate poor performance on segmentation of small objects segmentation. This can have significant impact on early detection of disease. This paper proposes a Context Axial Reserve Attention Network (CaraNet) to improve the segmentation performance on small objects compared with recent state-of-the-art models. We test our CaraNet on brain tumor (BraTS 2018) and polyp (Kvasir-SEG, CVC-ColonDB, CVC-ClinicDB, CVC-300 and ETIS-LaribPolypDB) segmentation. Our CaraNet not only achieves the top-rank mean Dice segmentation accuracy, but also shows a distinct advantage in segmentation of small medical objects.

**Keywords:** Small object segmentation; Brain tumor; Colonoscopy; Attention; Context axial reverse

## Description of Purpose

Recently, various convolutional neural networks (CNNs) have shown great performance on medical image segmentation [1,2,3,4]. Most CNNs, however, focus on increasing the overall segmentation performance without regard to the segmentation performance on small medical objects. To detect small medical objects is very important for disease early detection and to reduce mortality. For example, for the brain tumor, the survival rate will decrease with the growing size of brain tumor [20]. Therefore, it is important to detect tumors when they are small. Although many neural networks show good performance on medical image segmentation, they suffer from high missed-detection rates when segmenting small medical objects. To solve this problem, we propose here a novel attention-based deep neural network, called **Context Axial Reverse Attention Network (CaraNet)**. The contribution of the paper can be summarized as follows:

- 1) We propose a novel neural network – CaraNet -- to solve the problem of segmentation of small medical objects.
- 2) We introduce a method to evaluate the network's performance on small medical objects.
- 3) Our experiments show that CaraNet outperforms most current models (e.g., PraNet from MICCAI' 20) and advances the state-of-the-art by a large margin, both overall and on small objects, in segmentation performance on polyps.

## Method

Figure 1 shows the architecture of our CaraNet, which uses a parallel partial decoder [4] to generate the high-level semantic global map and a set of context and axial reverse attention operations to detect global and local feature information. We will introduce each component in the following subsections.

### A. Parallel partial decoder

Currently, most popular segmentation models are based on the U-Net, which aggregates all level feature maps from encoders. Experiments have shown that, low-level features are more computationally costly but contribute less to improve segmentation performance [5]. So, we used a parallel partial decoder to aggregate high-level features. As shown in Figure 1, we apply Res2Net [6] as a backbone network to extract low- and high-level features. And we apply a partial decoder  $p_d(\cdot)$  [5] to aggregate the high-level features. The partial decoder feature is computed by

$PD = p_d(f_3, f_4, f_5)$ , and we can get a global map  $S_g$  from the partial decoder.

## B. Context module

To get contextual information from high-level features, we apply a **Channel-wise Feature Pyramid** (CFP) module to obtain multi-scale feature information [7]. We set the dilation rate of CFP  $d = 8$ , so the dilation rate for each channel is  $\{1, 2, 4, 8\}$ . After the context module, we can obtain multi-scale high-level features  $\{f'_3, f'_4, f'_5\}$ .

## C. Axial reverse attention

The axial reverse attention module contains two parts: axial attention route and reverse attention route. The global map  $S_g$  could only capture only an approximate location of the tissues, without structural details. Therefore, we progressively mine discriminative tissue region through an erasure of the foreground object by applying reverse attention [8]. The reverse operation can be represented as:

$$R_i = 1 - \text{Sigmoid}(S_i) \quad (1)$$

For another route, we use axial attention to keep the global connection and for efficient computing [9]. In axial attention, the network can extract global dependencies and local representation by computing for both horizontal and vertical axes. And the output of A-RA module can be represented as:

$$ARA_i = AA_i \odot R_i \quad (2)$$

where  $\odot$  is element-wise multiplication and the  $AA_i$  is feature from the axial attention route.

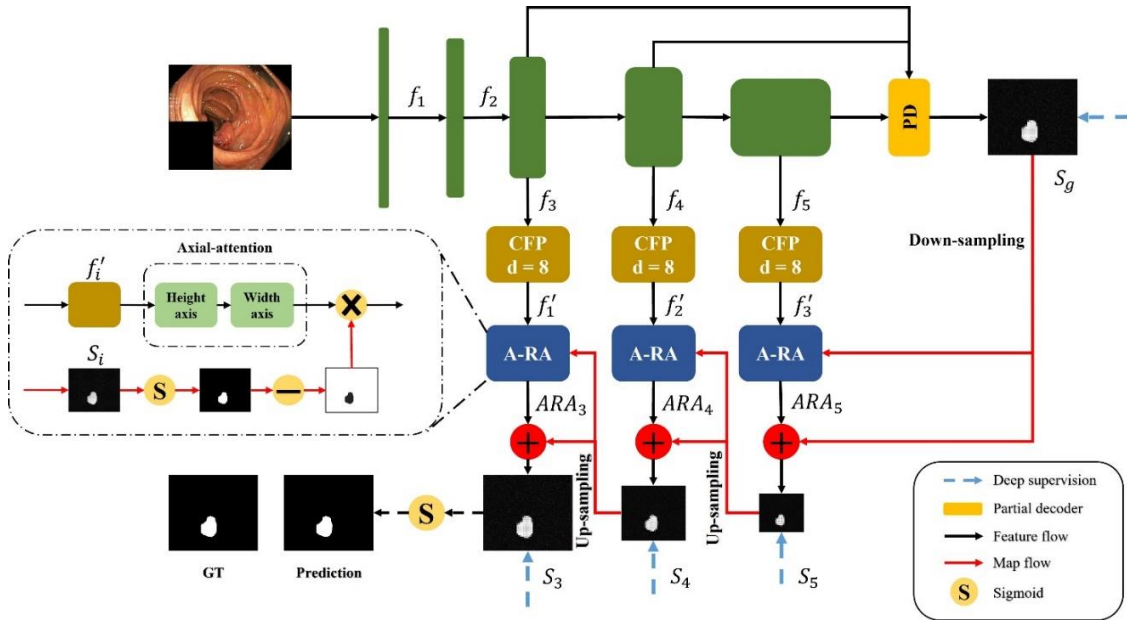


Figure 1. Overview of CaraNet, which contains three context modules (CFP) and axial reverse attention modules (A-RA). The ‘S’ is sigmoid function.

## D. Deep supervision

We apply weighted intersection over union (IoU) and weighted binary cross entropy (BCE) as our loss function to calculate the global loss and local (pixel-level) loss. The loss function can be represented as  $\mathcal{L} = \mathcal{L}_{IoU}^w + \mathcal{L}_{BCE}^w$ . To train CaraNet, we apply deep supervision for the three side-outputs ( $S_1, S_2, S_3$ ) and the global map  $S_g$ . Before calculating the loss, we up-sampled them to the same size as ground truth  $G$ . Thus, the total loss can be represented as:

$$\mathcal{L}_{total} = \mathcal{L}(G, S_g^{up}) + \sum_{i=3}^5 \mathcal{L}(G, S_i^{up}) \quad (3)$$

## E. Small object segmentation analysis

The size of an object is determined by the number of pixels in the object and the size of the whole image because the

size of all images input to the segmentation models must be fixed. Thus, we consider the object's size using the ratio (proportion) of the number of pixels in the object to that of the whole image. Then, we evaluate the performance of segmentation models according to the sizes of objects. Especially, we focus on the small areas: those having proportions that are smaller than 5%.

For a segmentation model, we first obtain the mean Dice coefficients of test data. Similar to computing the histogram, we divide the entire range of size values of objects in test data into a series of intervals, which are consecutive, non-overlapping, and of equal length, and then calculate the average of mean Dice coefficients of data whose size values fall into each interval. The interval-averaged coefficients have a smooth curve and are more stable in the presence of noise.

## Results

### A. Experiments on polyp segmentation.

We choose five polyp datasets: ETIS [10], CVC-ClinicDB [11], CVC-ColonDB [12], EndoScene [13] and Kvasir [14]. We compare our CaraNet with six state-of-the-art medical image segmentation methods: UNet [1], U-Net++ [2], ResUNet-mod [15], ResUNet++ [3], SFA [16] and PraNet [4]. We randomly select 80% images from Kvasir and CVC-ClinicDB as training set and the remainder as a testing dataset. In addition to mean Dice and mean IoU, we also select other four measurement metrics: weighted dice metric  $F_B^w$ , MAE, enhanced alignment metric  $E_\phi^{max}$  [17] and structural measurement  $S_\alpha$  [18]. Table 1 show the polyp segmentation on the five datasets.

Table 1. Quantitative results on Kvasir, CVC-ClinicDB, CVC-ColonDB, ETIS and CVC-T (test dataset of EndoScene).

Methods	mean Dice	mean IoU	$F_B^w$	$S_\alpha$	$E_\phi^{max}$	MAE
Kvasir	UNet	0.818	0.746	0.794	0.858	0.055
	UNet++	0.821	0.743	0.808	0.862	0.048
	ResUNet-mod	0.791	n/a	n/a	n/a	n/a
	ResUNet++	0.813	0.793	n/a	n/a	n/a
	SFA	0.723	0.611	0.670	0.782	0.075
	PraNet	0.898	0.840	0.885	0.915	0.030
	CaraNet	<b>0.918</b>	<b>0.865</b>	<b>0.909</b>	<b>0.929</b>	<b>0.023</b>
CVC-ClinicDB	UNet	0.823	0.755	0.811	0.889	0.019
	UNet++	0.794	0.729	0.785	0.873	0.022
	ResUNet-mod	0.779	n/a	n/a	n/a	n/a
	ResUNet++	0.796	0.796	n/a	n/a	n/a
	SFA	0.700	0.607	0.647	0.793	0.042
	PraNet	0.899	0.849	0.896	0.936	0.009
	CaraNet	<b>0.936</b>	<b>0.887</b>	<b>0.931</b>	<b>0.954</b>	<b>0.007</b>
Colon DR	UNet	0.512	0.444	0.498	0.712	0.061
	UNet++	0.483	0.410	0.467	0.691	0.064
	SFA	0.469	0.347	0.379	0.634	0.094
	PraNet	0.709	0.640	0.696	0.819	0.045
	CaraNet	<b>0.773</b>	<b>0.689</b>	<b>0.729</b>	<b>0.853</b>	<b>0.042</b>
ETIS	UNet	0.398	0.335	0.366	0.684	0.036
	UNet++	0.401	0.344	0.390	0.683	0.035
	SFA	0.297	0.217	0.231	0.557	0.109
	PraNet	0.628	0.567	0.600	0.794	0.031
	CaraNet	<b>0.747</b>	<b>0.672</b>	<b>0.709</b>	<b>0.868</b>	<b>0.017</b>
CVC-T	UNet	0.710	0.627	0.684	0.843	0.022
	UNet++	0.707	0.624	0.687	0.839	0.018
	SFA	0.467	0.329	0.341	0.640	0.065
	PraNet	0.871	0.797	0.843	0.925	0.010
	CaraNet	<b>0.903</b>	<b>0.838</b>	<b>0.887</b>	<b>0.940</b>	<b>0.007</b>

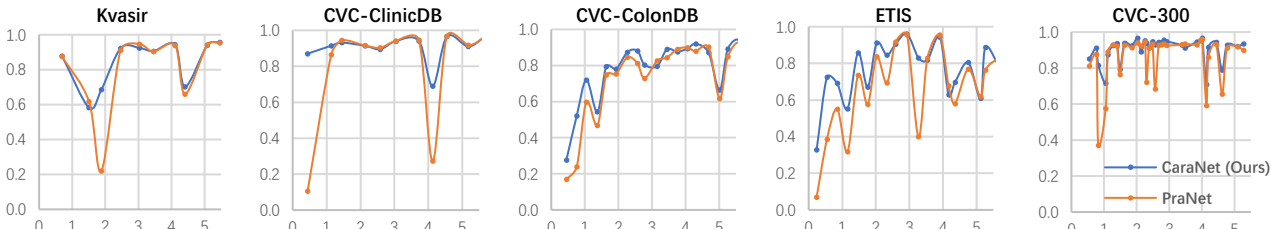


Figure 2. Performance vs. Size on the five polyp datasets. The x-axis is the proportion size (%) of polyp; y-axis is the averaged mean Dice coefficient. Blue is for our CaraNet and orange is for the PraNet.

For the five polyp datasets, our CaraNet not only outperforms compared models according to overall performance, but also

on samples with small size polyps. Figure 2 shows segmentation performance of CaraNet and PraNet for small objects (proportions  $\leq 5\%$ ). For the small object segmentation analysis, we compare our CaraNet only with PraNet because PraNet has the closest performance to ours, and the overall accuracies of the other segmentation methods are clearly lower than those of CaraNet and PraNet. (Note: the fluctuations with size in colonoscopy datasets are caused by types and boundary of polyps, and quality of imaging)

## B. Experiment on brain tumor segmentation

To further evaluate the effectiveness of CaraNet for small object segmentation, we conducted a different experiment, this time using the brain tumor (BraTS 2018) dataset. Because the polyp datasets lack extremely small objects (the minimum is about 0.11%) and do not have enough small samples (like Kvasir and CVC-ClinicDB, in Figure 2, there are fewer points in the range of small sizes). The brain tumor dataset was created from BraTS 2018 [19] database by slicing 2D images from the “T1ce” source with “NET” type labels. We randomly select 60% images as training set and the remainder as the testing dataset. Altogether, 3231 images with proportions of tumor sizes ranging from 0.01% – 4.91% were in the testing dataset. Table 2 and Figure 3 show the comparison result. We compared CaraNet with only PraNet for the same reason stated above. Clearly, our CaraNet performed better, especially for the extremely small cases (range 0.01% – 0.1% in Figure 3).

Table 2. Quantitative results on brain tumor (BraTS 2018) dataset.

Methods	mean Dice	mean IoU	$F_R^w$	$S_\alpha$	$E_{\phi}^{max}$	MAE
CaraNet (Ours)	0.631	0.507	0.629	0.786	0.927	0.003
PraNet (MICCAI'20)	0.619	0.494	0.606	0.776	0.920	0.003

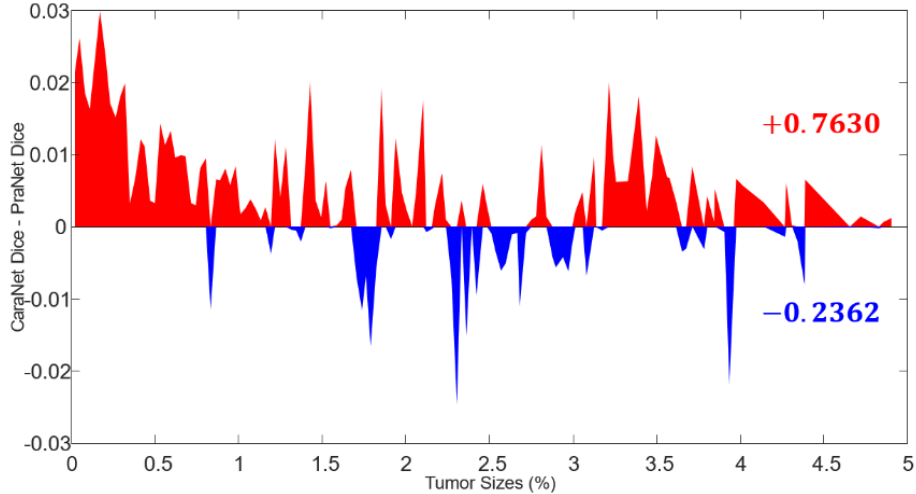


Figure 3. Performance vs. Size on brain tumor datasets. The x-axis is the proportion size (%) of tumor; the y-axis is the difference between the averaged mean Dice coefficient results of CaraNet and PraNet. Red indicates the Dice value of CaraNet is greater than that of PraNet; blue shows the opposite. Values on the right show the summations of all red and blue differential values.

## New or breakthrough work to be presented

We propose a novel deep-learning based segmentation model – CaraNet, by combining the Axial Reverse Attention and Channel-wise Feature Pyramid (CFP) modules. This new method can help improve the performance of segmentation of small medical objects. Through the experiments, CaraNet outperforms most cutting-edge models and advances the state-of-the-art by a large margin overall, and small objects’ segmentation performance on polyps and brain tumors. We also introduced the process to evaluate segmentation models according to the size of objects.

## Conclusion

We have proposed a novel neural network, CaraNet, for small medical object segmentation. From the overall segmentation accuracy, we can find that CaraNet outperforms all state-of-art approaches by at least 2% (mean dice accuracy). For the early diagnosis dataset, ETIS, which contains many small polyps however, CaraNet can reach 74.7% mean dice accuracy, which is about 12% higher than PraNet.

## References

- [1] Ronneberger, O., Fischer, P., & Brox, T. (2015, October). U-net: Convolutional networks for biomedical image segmentation. In International Conference on Medical image computing and computer-assisted intervention (pp. 234-241). Springer, Cham.
- [2] Zhou, Z., Siddiquee, M. M. R., Tajbakhsh, N., & Liang, J. (2018). Unet++: A nested u-net architecture for medical image segmentation. In Deep learning in medical image analysis and multimodal learning for clinical decision support (pp. 3-11). Springer, Cham.
- [3] Jha, D., Smedsrud, P. H., Riegler, M. A., Johansen, D., De Lange, T., Halvorsen, P., & Johansen, H. D. (2019, December). Resunet++: An advanced architecture for medical image segmentation. In 2019 IEEE International Symposium on Multimedia (ISM) (pp. 225-2255). IEEE.
- [4] Fan, D. P., Ji, G. P., Zhou, T., Chen, G., Fu, H., Shen, J., & Shao, L. (2020, October). Pranet: Parallel reverse attention network for polyp segmentation. In International Conference on Medical Image Computing and Computer-Assisted Intervention (pp. 263-273). Springer, Cham.
- [5] Wu, Z., Su, L., & Huang, Q. (2019). Cascaded partial decoder for fast and accurate salient object detection. In Proceedings of the IEEE/CVF Conference on Computer Vision and Pattern Recognition (pp. 3907-3916).
- [6] Gao, S., Cheng, M. M., Zhao, K., Zhang, X. Y., Yang, M. H., & Torr, P. H. (2019). Res2net: A new multi-scale backbone architecture. IEEE transactions on pattern analysis and machine intelligence.
- [7] Lou, A., & Loew, M. (2021). CFPNet: Channel-wise Feature Pyramid for Real-Time Semantic Segmentation. arXiv preprint arXiv:2103.12212.
- [8] Chen, S., Tan, X., Wang, B., & Hu, X. (2018). Reverse attention for salient object detection. In Proceedings of the European Conference on Computer Vision (ECCV) (pp. 234-250).
- [9] Ho, J., Kalchbrenner, N., Weissenborn, D., & Salimans, T. (2019). Axial attention in multidimensional transformers. arXiv preprint arXiv:1912.12180.
- [10] Silva, J., Histace, A., Romain, O., Dray, X., & Granado, B. (2014). Toward embedded detection of polyps in wce images for early diagnosis of colorectal cancer. International journal of computer assisted radiology and surgery, 9(2), 283-293.
- [11] Bernal, J., Sánchez, F. J., Fernández-Esparrach, G., Gil, D., Rodríguez, C., & Vilariño, F. (2015). WM-DOVA maps for accurate polyp highlighting in colonoscopy: Validation vs. saliency maps from physicians. Computerized Medical Imaging and Graphics, 43, 99-111.
- [12] Tajbakhsh, N., Gurudu, S. R., & Liang, J. (2015). Automated polyp detection in colonoscopy videos using shape and context information. IEEE transactions on medical imaging, 35(2), 630-644.
- [13] Vázquez, D., Bernal, J., Sánchez, F. J., Fernández-Esparrach, G., López, A. M., Romero, A., ... & Courville, A. (2017). A benchmark for endoluminal scene segmentation of colonoscopy images. Journal of healthcare engineering, 2017.
- [14] Jha, D., Smedsrud, P. H., Riegler, M. A., Halvorsen, P., de Lange, T., Johansen, D., & Johansen, H. D. (2020, January). Kvasir-seg: A segmented polyp dataset. In International Conference on Multimedia Modeling (pp. 451-462). Springer, Cham.
- [15] Zhang, Z., Liu, Q., & Wang, Y. (2018). Road extraction by deep residual u-net. IEEE Geoscience and Remote Sensing Letters, 15(5), 749-753.
- [16] Fang, Y., Chen, C., Yuan, Y., & Tong, K. Y. (2019, October). Selective feature aggregation network with area-boundary constraints for polyp segmentation. In International Conference on Medical Image Computing and Computer-Assisted Intervention (pp. 302-310). Springer, Cham.
- [17] Fan, D. P., Gong, C., Cao, Y., Ren, B., Cheng, M. M., & Borji, A. (2018). Enhanced-alignment measure for binary foreground map evaluation. arXiv preprint arXiv:1805.10421.
- [18] Fan, D. P., Cheng, M. M., Liu, Y., Li, T., & Borji, A. (2017). Structure-measure: A new way to evaluate foreground maps. In Proceedings of the IEEE international conference on computer vision (pp. 4548-4557).
- [19] S. Bakas, M. Reyes, A. Jakab, S. Bauer, M. Rempfler, A. Crimi, et al. (2018). Identifying the Best Machine Learning Algorithms for Brain Tumor Segmentation, Progression Assessment, and Overall Survival Prediction in the BRATS Challenge. arXiv preprint arXiv:1811.02629 .
- [20] Ngo, D. K., Tran, M. T., Kim, S. H., Yang, H. J., & Lee, G. S. (2020). Multi-task learning for small brain tumor segmentation from MRI. Applied Sciences, 10(21), 7790.